JGR Atmospheres

The Representation of Föhn Events to the East of the Antarctic Peninsula in Simulations by the Antarctic Mesoscale Prediction System

Amélie Kirchgaessner[1], John King[1], and Alan Gadian[2,3]

[1]British Antarctic Survey, Cambridge, UK, [2]National Centre of Atmospheric Sciences, Leeds, UK, [3]School of Earth and Environment, University of Leeds, Leeds, UK

Abstract Föhn winds are warm, strong, downslope winds on the leeside of mountains, which can last from several hours to a few days. The years 1995 and 2002 saw the dramatic breakup of huge parts of the Larsen Ice Shelf (LIS) on the east of the Antarctic Peninsula. It is widely accepted that hydrofracturing, the widening of crevasses due to the excess hydrostatic pressure exerted by meltwater which accumulates inside them, is the mechanism behind the breakup of the Larsen A and Larsen B ice shelves. On the LIS, in the lee of the mountain range that runs along the spine of the Antarctic Peninsula, Föhn winds are thought to provide the atmospheric conditions for significant warming over the ice shelf, leading to the initial firn densification, and subsequently providing the melt water for hydrofracturing. Measurements provide evidence that in some cases Föhn events reach an Automatic Weather Station on the LIS at over 100 km distance. In this paper, we examine the representation of Föhn events during 2011 as they were observed in measurements by an Automatic Weather Station and in simulations with the Weather Research and Forecasting Model as run for the Antarctic Mesoscale Prediction System (AMPS). We find that, while the model generally simulates meteorological parameters very well and shows good skill in capturing the occurrence, frequency, and duration of Föhn events, it underestimates the temperature increase and humidity decrease during the Föhn significantly and may thus underestimate the contribution of Föhn to driving surface melt on LIS.

1. Introduction

Over the second half of the twentieth century the Antarctic Peninsula (AP) was one of the most rapidly warming parts of the planet (King et al., 2003; Turner et al., 2005; Vaughan et al., 2001). The strongest warming occurred on the western side of the peninsula during winter, while, in summer, warming was greatest on the eastern side (Marshall et al., 2006). As dramatic manifestations of this warming, Larsen A and B ice shelves disintegrated in 1995 and 2002, respectively. While these events do not directly affect sea level rise, ice shelves (ice beyond the actual coastline) act as buffers to the glaciers (ice on land) that feed them. Removing this buffer accelerates the discharge of glacial ice into the ocean, which, in contrast to shelf ice does contribute to sea level rise (Scambos et al., 2004).

The climate of the AP is strongly controlled by the circumpolar westerly winds that blow around the Southern Ocean. The strength and location of the circumpolar westerlies is determined by a roughly zonally symmetric pattern of pressure variability between Antarctica and midlatitudes, known as the Southern Annular Mode (SAM). These circumpolar westerlies only encounter one topographic barrier, the AP mountains. This mountain range forms the spine of the AP, with peaks over 2,000 m height and its north-south orientation forms an almost perpendicular barrier to the circumpolar westerlies around the Antarctic continent (Figure 1).

Three mechanisms can lead to Föhn events along the AP mountain range. When SAM is in a positive phase, the strengthened westerly winds can overcome barrier formed by the AP mountains, which can lead to thermodynamically driven Föhn. The basis for this is the difference between the generally warm, moist air on the western side of the AP, where there is little to no sea ice, and cold, dry air on the eastern side of the AP over the ice shelves. In a linear flow regime, when strong westerlies drive this warm, moist air up the slopes of this mountain range, the rising air undergoes adiabatic expansion and cools (initially at the dry
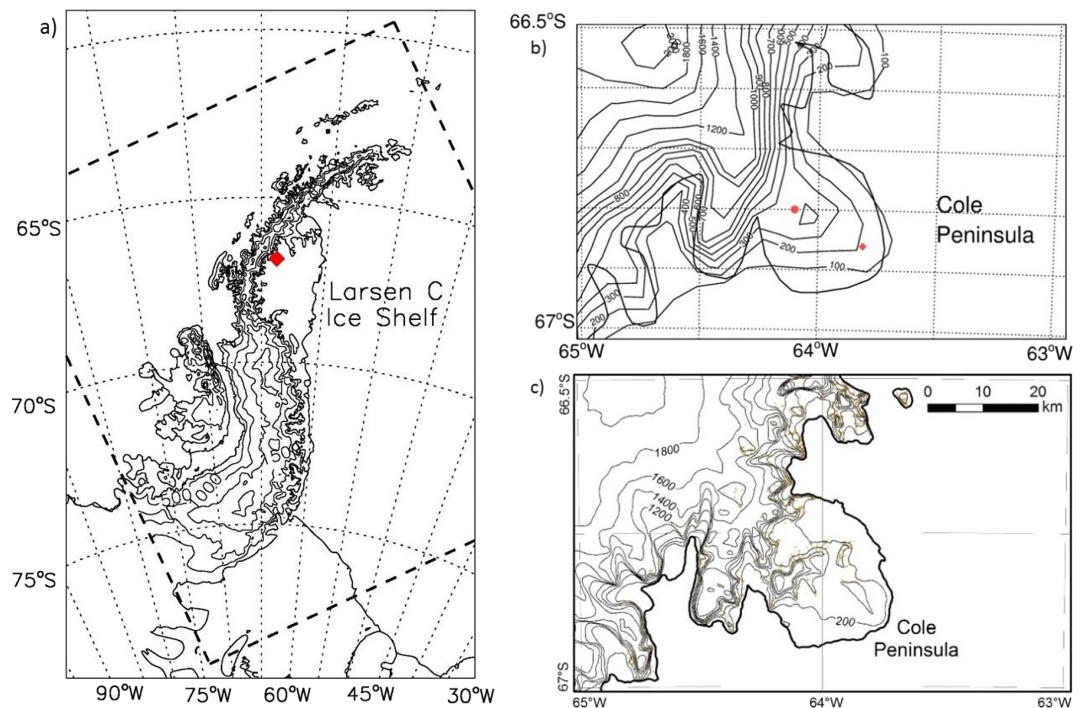
Figure 1. a) Map of Antarctic Peninsula, showing the location of the AWS on Cole Peninsula (red diamond) and the Larsen Ice Shelf. Bold dashed lines mark the borders of the 5 km resolution AMPS domain. b) The map on the top right shows a close-up of the coastline in the area of Cole Peninsula (based on survey data by the British Antarctic Survey's Mapping and Geographical Information Centre). Contours are based on the orography used in AMPS. The red diamond marks the actual geographic coordinates of the AWS, and the red circle marks the model location used for comparison in this study. c) Orography in the area of Cole Peninsula based on survey data by the Mapping and Geographical Information Centre of the British Antarctic Survey. Contour lines are in 250 m, and shaded contours mark 300 ft.

adiabatic lapse rate) and eventually reaches saturation point. Subsequent condensation and precipitation removes moisture and leads to irreversible latent heating (Beran, 1967; Smith, 1990), and means the air, while still rising on the windward side, continues to cool at the lower moist adiabatic lapse rate. During its descent on the leeside of the mountains, the air undergoes adiabatic compressional heating and warms at the dry adiabatic lapse rate. The resultant air on the leeside is thus warmer and drier than that on the windward side (Orr et al., 2008). Model results by van Lipzig et al. (2008) are consistent with this mechanism, showing increased cloud cover, surface mass balance (which correlates with precipitation), and cloud ice/water to the west of the AP during periods of positive SAM (SAM+) conditions, that is, stronger westerly circumpolar winds. A second dynamic mechanism for Föhn warming is isentropic drawdown in a nonlinear flow regime. This occurs when air is sourced from higher altitude upwind of the topographic obstacle as a result of upwind flow blocking at a level below the ridge crest. In a stably stratified atmosphere this air will be potentially warmer and usually drier than the air below (Richner & Hächler, 2013; Smith, 1990). A third mechanism observed in the lee of the AP that can lead to warmer, drier air at low level is a combination of mechanical mixing and radiative heating (Elvidge & Renfrew, 2016).

Between approximately 1965 and 2000, the SAM exhibited a distinct trend to a more positive polarity (i.e., stronger westerlies), thought to be a product of anthropogenic forcing (Marshall, 2003). Marshall et al. (2006) then identified a strong correlation between the summer surface warming on the eastside of the AP and the positive trend in the SAM, which is largest during summer and autumn (Marshall, 2003). A regional mechanism to explain this relationship was proposed, whereby the strengthened westerlies drive enhanced air flow over the peninsula, thus inducing strong leeside downslope Föhn winds and adiabatic warming on the eastside (Elvidge et al., 2015; Orr et al., 2008). Cape et al. (2015) confirmed that the positive trend in SAM is reflected in a significant increase in the occurrence of Föhn winds in summer over Larsen B Ice Shelf.

An increased frequency and/or intensity of Föhn winds, caused by strengthened westerlies, is thought to have provided the necessary atmospheric conditions for prolonged periods of melt in the lee of the AP over the Larsen Ice Shelf (LIS). These in turn have led to firn densification and subsequently provided the melt water for hydrofracturing (Cape et al., 2015; Kuipers Munneke et al., 2014; McGrath et al., 2012). Hydrofracturing, that is, the widening of crevasses due to the excess hydrostatic pressure exerted by intruding meltwater, is generally accepted as the mechanism behind the collapse and breakup of Larsen A and Larsen B ice shelves (Banwell et al., 2013; Scambos et al., 2003). The remaining part of the LIS, Larsen C Ice Shelf (LCIS), stretches roughly from 65.2°S to 65.8°S and, bound in the west by the AP, reaches eastward to approximately 61°W (Figure 1). Other mechanisms that can contribute to the disintegration of ice shelves are the decline in sea ice and increased exposure to ocean swell (Massom et al., 2018).

Observations have shown the important role that Föhn-induced melt plays for the structural integrity of ice shelves along the eastern side of the AP. The sparsity of observations, however, limits our ability to reliably predict future behavior under changing climate conditions. To better understand and reliably predict the future behavior of LCIS, it is essential that models used for investigating and forecasting melt are able to simulate the atmospheric conditions that may lead to melt correctly and represent the components of the surface energy balance realistically. This paper investigates whether a regional atmospheric model can accurately simulate the occurrence and characteristics of Föhn conditions in the region of the AP. We are using the data from the Antarctic Mesoscale Prediction System (AMPS) at 5 km resolution. By comparing model simulations with observational data, we identify where the model exhibits difficulties in representing Föhn conditions adequately. We attempt to find explanations for weaknesses in the model simulations of Föhn and explore approaches to possible solutions for model improvement.

2. Data and Methods

2.1. Automatic Weather Station Data

In this study we use observational data from an Automatic Weather Station (AWS) that was deployed on the eastern side of the AP, on Cole Peninsula (CP), on 21 January 2011 as part of a field experiment focusing on the influence of the AP's orography on the regional climate. It was installed at 66.86°S, 63.81°W and at 424 m above sea level (Figure 1). To deploy the AWS on the ice shelf at Mill Inlet just south of CP was not safely possible due to heavy crevassing. The coastline in the region of the LIS is characterized by a sequence of jagged peninsulas and inlets. CP reaches out into the LCIS by about 80 km. At its eastern end, it forms an almost circular and relatively flat plateau of about 50 km diameter. This rises steeply from the ice shelf to a height of about 250 m. Embedded in this plateau are features of over 750 m. To the west and the north of CP, the terrain quickly rises up to the Avery and Bruce Plateaus, which reach heights of 1,700 m above sea level and more. We do not include AWSs further east on the LCIS, as Föhn air becomes modified as it flows away from the mountains, and the signal weakens (Turton et al., 2018). Instead, we restrict our analysis to the observations from the AWS at CP, close to the foot of the mountains, where the clearest Föhn signal is found.

The AWS measured wind speed, ff, and direction, dd, with a Young propeller-vane anemometer (model 05103); temperature, T, and relative humidity, RH, with a Vaisala Humicap (HMP45); and absolute air pressure, p, by microelectromechanical sensor (SCP1000). Measurements were logged at 0.1 Hz and aggregated to 10 min mean values. These were stored on a separate memory card and transmitted via Iridium satellite communication about every 12 hr to an ftp-server at the British Antarctic Survey in Cambridge. A solar panel, with a lead-acid battery as backup, provided the power for the system. Instruments were mounted on an aluminum pole, with the anemometer at the top at ~4 m above the surface at the time of deployment and the Humicap about 0.5 m below this. The pressure sensor was incorporated into the logger box, which was buried about 0.5 m deep in the snow at the foot of the pole. Anderson et al. (1992) have shown that a pressure sensor buried in porous snow or firn is adequately ventilated. Furthermore, burying the box with the pressure sensor has the advantage to remove spurious pressure fluctuations associated with wind fluctuations. The AWS was revisited for maintenance on 14 December 2011. Possibly due to intruding melt water after the maintenance, the AWS stopped working reliably on 4 January 2012. About 0.5 m of snow had accumulated at the location between deployment and the maintenance visit. It was retrieved on 20 February 2012 by British Antarctic Survey staff.

We calibrated T measurements according to a predeployment calibration. Values of RH were adjusted to saturation over ice for below-freezing temperatures. To extend the calibrated range of the RH sensor for very low air temperatures, we used the method described by Anderson (1994). Wind direction values were adjusted to a compass bearing taken during installation of the AWS. The AWS data were further averaged into centered 6-hourly values for 3, 9, 15, and 21 UTC. This brings the AWS data onto the same temporal resolution as the available model data (see next section). Further, we have analyzed the hourly observational data for Föhn events, which have shown that in the overwhelming majority of cases (96%) Föhn conditions persist for 6 hr or more. Therefore, we are confident that this reduction in temporal resolution does not compromise the robustness of our results. The period under consideration in this study starts on 22 January 2011 and finishes at the end of the year on 31 December 2011. This includes 344 days of potential data and—with regard to 6-hourly data used here—1,376 potential data points. As, during some periods, data transmission from the AWS failed, the actual number of available 6-hourly data points is 1,352, equating to a net loss of one complete day of observations.

2.2. The AMPS

In this study, we evaluate the representation of Föhn events by the AMPS. AMPS (Powers et al., 2012) is a numerical weather prediction system for the Antarctic region, run operationally by the Mesoscale and Microscale Meteorology Division of the National Center for Atmospheric Research in Boulder, Colorado, USA. It is a web-based repository that provides support for the United States Antarctic Program, Antarctic science, and international Antarctic efforts (Powers et al., 2003). AMPS is an operational system serving multiple purposes and consequently numerous constraints. A higher spatial resolution may have been desirable for this application, but AMPS has to run on available computer cycles within a tight time window to be useful for forecast purposes. This limits the spatial resolution that can be used for the AP domain.

For the period under investigation, AMPS used the nonhydrostatic Weather Research and Forecasting model (WRF) v3.0.1 with modifications to improve the representation of the surface energy balance over permanently ice-covered regions. This model configuration is commonly referred to as Polar WRF (Hines & Bromwich, 2008; Skamarock, 2008). It uses the Rapid Radiative Transfer Model longwave radiation scheme and the Goddard shortwave radiation scheme. Surface fluxes are calculated using the Eta similarity scheme, based on Monin-Obukhov similarity theory. The boundary layer is represented by the Mellor-Yamada-Janjic scheme (Janjic, 1994). Cloud microphysical properties are calculated using the WRF single-moment Class 5 (WSM5; Hong et al., 2004) scheme.

The model was run on a series of two-way nested domains with 44 vertical levels between the surface and the model top (10 hPa). In this setup the lowest model level was roughly 16 m above the surface, and there were 12 levels in the lowest 1 km. The outermost (45 km resolution, 220×290 points) domain covered Antarctica and much of the Southern Ocean. A nested 15 km resolution (442×418 points) domain covered the Antarctic continent and, within this, a 5 km resolution (346×301 points) domain covered the AP region. Data from this innermost domain are used in this study. The Global Forecast System 0.5° numerical weather prediction system run by the U.S. National Centers for Environmental Prediction provided lateral boundary conditions for the outer (45 km) domain, which were updated every 6 hr. Observations within the AMPS domain were assimilated using a 3-D variational data assimilation scheme. The AMPS system was run twice a day, starting from Global Forecast System analyses valid at 0000 and 1200 UTC. Forecasts for the 5 km AP domain were run to $T + 36$ hr for each of these initialization times. After having served its purpose as weather forecasting tool, the hourly model output is stored in the AMPS Archive. Through this archive, the data are subsequently available for the scientific community for studies like this present one and are accessible online (https://www.earthsystemgrid.org/).

Constraints on data transfer and storage, together with considerations of the topic under investigation, led to the decision to only use 6-hourly model output from the archive, and restrict the analysis to forecasts up to $T + 24$, which, we believe, has not changed the results. At 5 km resolution, the model representation of the complex terrain in the area is significantly smoothed. This leads to a substantial difference between the model terrain and reality with regard to height above sea level at the location of the AWS. Due to the model's resolution and orography in the area, the geographical location of the CP AWS in the model (interpolated from surrounding grid points) is represented by a point that is 186 m above sea level—more than 200 m below the real height at this location. Taking the model's land-sea mask and topography into account, a

location was selected (see Figure 1) that better represents the actual topography of the real AWS location. The point chosen to represent the "model" location of the AWS for this study is 66.8°S and 64.1°W. The model topography at this pseudo AWS location gives it a height of 391 m above sea level, 35 m below the actual altitude of the AWS. Model data were bilinearly interpolated to this location for comparison with AWS measurements.

We extracted those parameters from the model output that were required for the closest possible comparison with the standard meteorological variables measured by the AWS. By combining forecast products after 12 (f12) and 18 hr (f18), alternating from initializations at 00 and 12 UTC, we created an artificial time series with values at 00, 06, 12, and 18 UTC. To give the model atmosphere time to fully adjust to the high-resolution topography and land surface, we disregarded the first 11 hr of model output (Seefeldt & Cassano, 2008; Steinhoff et al., 2009). To make the modeled values representative for the synoptic situation rather than a certain point in time, they were averaged to match the centered averages of the AWS observations at 03, 09, 15, and 21 UTC.

For comparison with AWS measurements we extracted 1.5 m temperature and surface pressure. For the comparison with observed RH, the water vapor mixing ratio q, surface pressure, and air temperature at 1.5 m were used to calculate RH2m. To compare an absolute measure of the air's moisture content, the absolute humidity was also calculated from the AWS and the AMPS data. Wind speed and wind direction were compared using model output of u and v at 10 m above surface, as these are the values closest to the surface that are available from the model.

2.3. Identification of Föhn

Föhn identification in AMPS and AWS comprised the core of our data analysis. We will refer to individual data points that fulfil Föhn criteria as Föhn, or as showing Föhn conditions, and an uninterrupted sequence of qualifying data points as a Föhn event. Separate Föhn identification criteria were used for AWS and AMPS data. We describe the two different methods in the next two paragraphs.

Data points in the AWS time series had to fulfil a set of criteria to be classified as Föhn. We chose RH rather than T as the main criterion, as the generally high air temperature during summer months can often mask the Föhn signal in T. The Föhn-related change in RH on the other hand is clearly distinguishable all year round (Figures 2, 3a, and 3b). Times when RH was equal or lower than 65% were declared to show Föhn conditions. This threshold was derived from assessing Föhn events in CP AWS observations during an intensive field campaign by aircraft. This is the same campaign the paper by Elvidge et al. (2015) is based on. This simple criterion sometimes missed short-lived, or less pronounced Föhn conditions, often prior to or after periods of intensive and persisting Föhn conditions. To include these cases, times were also identified as Föhn, when RH was 70% or lower and the temperature increased by at least 3 K in the previous 12 hr or decreased by at least 3 K over the following 12 hr. We derived these thresholds from obvious Föhn cases that had been missed by the simple "RH only" criterion. Two case studies that exemplify this are presented as supplementary material to this paper (Figure S1 in the supporting information). The most obvious criterion for Föhn identification—a downslope westerly wind—proved to be an unreliable indicator in our observational data set, likely due to local topographic influences on the measurements of wind direction at the AWS (Figure 1c).

These criteria are similar to those applied by other studies investigating Föhn in Antarctica (Speirs et al., 2010; Steinhoff et al., 2014) and elsewhere (Gaffin, 2007; Richner et al., 2006). While Speirs et al. (2010) and Steinhoff et al. (2014) base their identification on the rate of change of T and RH, their identification is based on 15 min measurements. Using averages over 6 hr as in this study leads to comparable rates of change for both RH and T. Gaffin (2007) uses differences in daily maximum air temperature to neighboring stations that are not under the influence of the Föhn, a method that is not available to us, owing to the availability of only this one isolated AWS. Richner et al. (2006) use a very similar approach to the one used in this paper; a (semi)automated Föhn diagnosis, based on a wind index which combines speed and directional information, together with anomalies of temperature and relative humidity. As in this paper, their threshold values are adjusted to individual stations.

To identify Föhn conditions in the AMPS data, we used a slight modification of the method described by King et al. (2017). This method uses the "drawdown" of isentropes (contours of potential temperature) in the lee of the AP mountains as a marker for Föhn conditions.
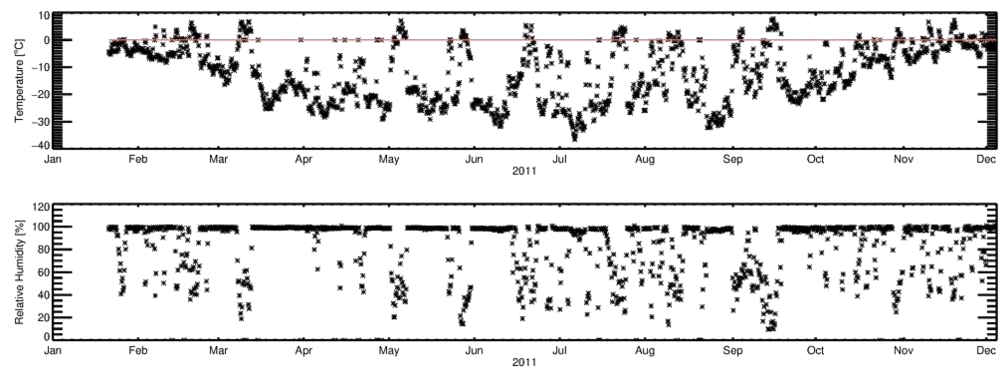
Figure 2. The 6-hourly observed *T* (upper panel) and observed *RH* (lower panel) in 2011 at Cole Peninsula AWS.

The potential temperature at 70°W (i.e., on the windward side of the mountain range), at 2,000 m height (chosen considering the height of the mountain range at this latitude), and 66.8°S (to match the latitudinal coordinate of the model location used for the comparison with the AWS) was extracted from the model output. The point at 70°W is about one Rossby radius upwind of the AP and therefore can be considered representative of the undisturbed upwind flow under westerly conditions. Then the minimum height of this potential temperature value on the leeside of the mountains along 66.8°S was determined in the section between 64°W and 66°W. If this minimum height was lower than 1,500 m (signifying a drawdown of at least 500 m), this data point was classified as Föhn. This longitudinal section was chosen empirically to cover the area on the leeside of the mountain range which may be influenced by Föhn winds while minimizing the risk of including cases when an increased near surface temperature is caused by other causes than Föhn. All parameters in this method are specifically chosen for this latitude, and would have to be adapted, when applying this algorithm to data from any other latitude along the AP, according to the slightly curved shape of the mountain range and the varying height of the summits.

The combination of these two Föhn identification methods allows us to identify initially the near surface signature of potential Föhn in the AWS data, and then—using the AMPS algorithm—to confirm whether this signal is really connected to Föhn flow. We use the model here not as "truth" but in lieu of additional observations in the region. This approach allows us, for example, to eliminate cases when a Föhn-like signature was found in the observations, which was caused by advection of warm air from the north east when a cyclone had formed at the tip of the AP. It also eliminates cases when AMPS incorrectly fails to simulate Föhn, for example, due to a timing error. Hence, we are only validating AMPS for cases when we know that AMPS (correctly) simulated Föhn. Not applying thresholds to the AMPS data set has the further advantage that it will not bias any validation of the model's capability to capture and represent Föhn characteristics in *T* and *RH*.

Only points in time that are classified as Föhn by both algorithms are considered as Föhn in the context of this study. Points in time that do not fulfil the Föhn criteria by both algorithms (i.e., in both data sets) are referred to as "no Föhn." Points in time, for which the two algorithms disagree in their classification, are discarded when categories of "Föhn" or no Föhn are analyzed but are included when the general meteorological and climatological characteristics at the location is described. We have done this for two reasons. First, it allows a clear distinction between Föhn versus non-Föhn conditions, and when comparing observations of Föhn with their simulations, we actually compare like with like. Second, this approach allows us to evaluate in how far the model simulates the onset, duration, and conclusion of Föhn conditions satisfactorily. Those points in time that were identified as Föhn by both algorithms were subsequently verified by visually inspecting the large-scale flow patterns based on ERA-Interim reanalysis fields of the geopotential height of the 850 hPa level for westerly flow in the region of the AP mountains and the LIS.

3. Results

3.1. Quality of Föhn Identification

The two Föhn identification algorithms applied to the AWS and AMPS data, respectively, agree in identifying Föhn on 224 of the 1,352 data points (17%) and agree on identifying no Föhn conditions on 774 occasions
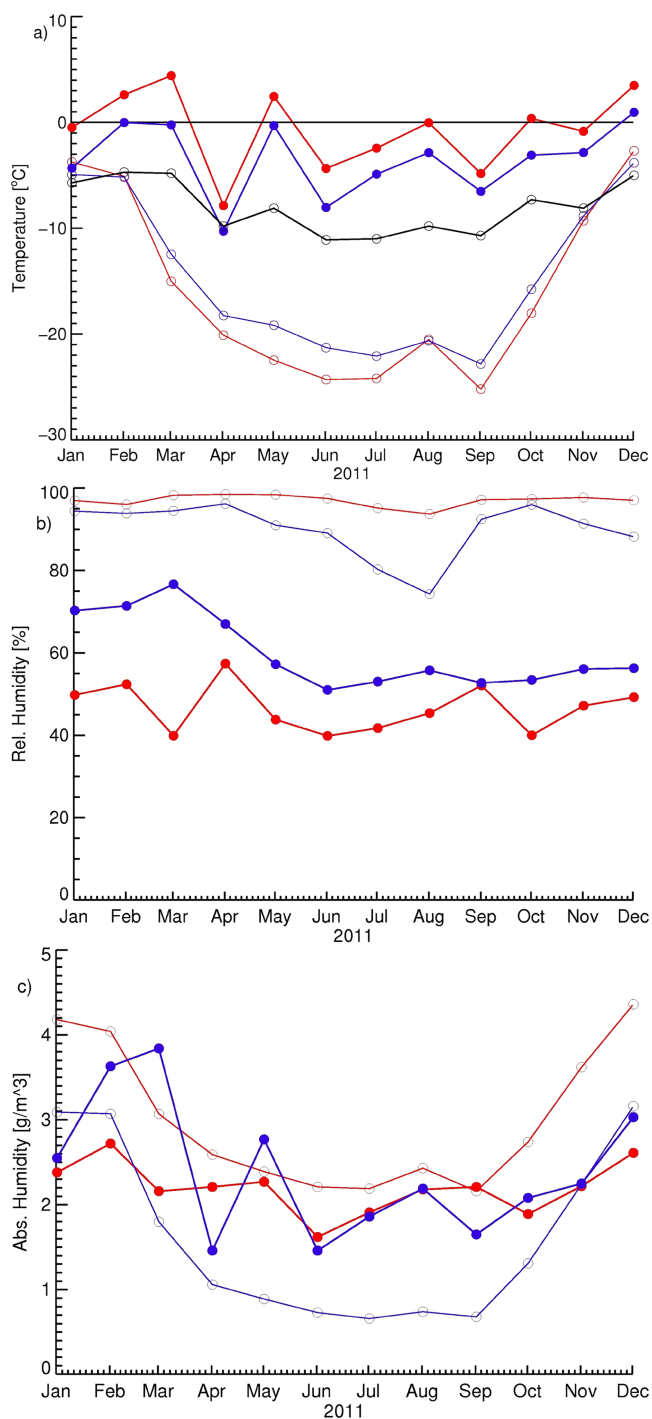
Figure 3. Monthly mean value of T (a), RH (b), and absolute humidity (c) from observations (red) and model data (blue) for Föhn (filled symbols) and non-Föhn (open symbols) composites. T and RH were measured at ~3.5 m above the snow surface. For T values below 0 °C, RH has been adjusted to saturation above ice. The black line on part (a) shows monthly mean temperatures at 65.56°S, 66.89°W, and 1,000 m from the ERA-Interim reanalysis.

(57%). We remind the reader that each of these points represents a discrete 6 hr time step. This corresponds to an agreement in 74% of all cases. They disagree in their classification on 354 occasions (26%), with 234 cases being classified as Föhn only in the AMPS data and by the respective algorithm and 120 cases being classified as Föhn by the AWS data and the respective algorithm only. Most of these cases are due to timing issues, that is, when Föhn conditions prevail for more than 6 hr, the onset and/or end of the Föhn event appear in one of the data sets earlier or later than in the other. There is no pattern to these discrepancies between the observation and simulation of onset and cessation of Föhn. Figure S2 in the supporting information gives an overview of the Föhn events as observed and simulated. The second most frequent reason for the algorithms to disagree is due to the signal being strong enough to meet Föhn criteria in one data set but not the other. This may mean that some valid Föhn cases are missed in the following analyses, but it allows a clear distinction between Föhn cases and non-Föhn cases, which is valid for both data sets.

3.2. Overall Comparison of Measurements and Model Data

Table 1 gives an overview of the general meteorological conditions during the period under investigation at CP. Mean values and standard deviations of T, p, RH, u, v, and ff are presented for observations and simulations. The table also contains the bias between observed and simulated data.

We performed t tests to determine whether the means of the observations and simulations of p, T, RH, u, v, and ff differ significantly. For Föhn conditions and non-Föhn conditions alike the observed and simulated means for T, RH, u, v, and ff are significantly different. The data sets do not differ significantly for p. All significances reach the 99% level, apart from T and u during non-Föhn conditions, when the difference between observations and simulations is only significant at the 95% level. The observed T at CP varied between −36.6 °C on 21 July and +7.8 °C on 6 October during a Föhn event. In the simulated data T ranges from −36.3 °C also on 21 July to +3.4 °C on 23 February during a Föhn event. Over the period under investigation, which covers almost one entire year, the model overestimates the near-surface temperature by almost 0.5 K.

RH values in the observations range from 10% to 100%. In the model simulations, values range from 14% to 110% (with respect to ice). The lowest value in the observational and simulation data set, respectively, occurs at different times. The respective other data set shows very dry conditions at the same time, too, albeit not to the same extent. The model underestimates RH on average by 3%. The influence of higher temperature and lower air pressure in the simulated data on similar moisture content alone cannot explain this discrepancy. The average u component of the wind in the measurement data, +1.6 m/s, is less than half that simulated by the model (+3.8 m/s). The mean scalar wind speed reflects this, being significantly lower in the measurements (3.9 m/s) than in the simulations (6.6 m/s). In the v component, the wind speed from measurements and simulations are more similar in magnitude (−1.9 and +1.2 m/s, respectively), but of opposite sign. This leads to a mean wind direction of north-west (319°) in the observational data and of west-south-west (252°) for the model data. This confirms that the area under investigation is clearly influenced by the circumpolar westerlies around the Antarctic continent. The discrepancy in the v component of the wind,

Table 1

Average Values, Standard Deviations, and Biases (Model Minus Observations, Bottom Row) of Standard Meteorological Parameters as Observed by the AWS at CP, and as Simulated by AMPS for all 1,352 Data Points

$n = 1{,}352$	T (°C)	p (hPa)	RH (%)	u (m/s)	v (m/s)	ff (m/s)
AWS	-12.3 ± 10.3	942.7 ± 11.9	84 ± 23	1.5 ± 4.2	-1.8 ± 1.7	3.9 ± 3.3
AMPS	-11.8 ± 8.6	942.5 ± 12.2	81 ± 19	3.8 ± 4.5	1.2 ± 4.9	6.6 ± 4.7
Mean bias	0.5	-0.2	-2	2.3	3.0	2.7
Correlation	**0.93**	**0.99**	**0.76**	**0.28**	-0.07	**0.49**
RMSE	3.88	1.59	15.6	5.68	6.07	5.05

Note. Correlations in bold are significant at the 99% level. *RH* values for AMPS are calculated for the lowest model level, and with surface near model output.

which leads to the model simulating a more southerly component while the measurements show on average a northerly component to the wind direction, may to some extent be attributed to local effects at the location of the AWS, which the model at 5 km resolution cannot be expected to reproduce. The model overestimates ff by 2.7 m/s, which is mainly caused by an overestimation of u. With regard to the average wind direction, the model simulations show a tendency for more southerly wind, while the measurements on average show a northerly component.

To compare further how observations and simulations represent the conditions, we calculated correlation coefficients for T, p, RH, u, v, and ff. Values are presented at the bottom of Table 1 together with the bias and the root-mean-square error. Modeled and observed temperatures are highly correlated ($r = 0.93$ for 6-hourly data and $r = 0.95$ for daily mean values). Correlations of the T anomalies from monthly means, to reduce the influence of the annual cycle, lead to correlation coefficients of 0.80 for the 6-hourly data. The high level of agreement between simulation and measurements of p presented above is also reflected in the correlation coefficient between the two data sets of 0.99. A correlation of 0.76 for RH is also remarkably good, given that the actual parameter is not direct model output, but is calculated from three modeled parameters, p, T, and q. The correlation coefficient for ff is 0.49, but those for the wind components are much lower (u: 0.28, v: -0.07).

The simulations generally follow the observations very well. The lowest temperature occurs in both data sets on the same day, if not at the same time. The highest temperature in both data sets occurs during Föhn events. However, while the highest temperature in the measurements is recorded during an event in October, the highest simulated temperature is associated with a Föhn event in February. Both Föhn events are identified as such in the measurement and model data, but differ in strength in the two data sets. The dry bias in the model is small in comparison to the dry bias of 10% points found by Wille et al. (2016) in their comparison of tower measurements near McMurdo with AMPS for a similar period. This is in contrast to other studies, for example, Fogt and Bromwich (2008) and Vázquez and Grejner-Brzezinska (2013), who reported a moist bias for AMPS across Antarctica. The overestimation of the wind speed is higher than that reported by Wille et al. (2016), but generally agrees with previous studies (Hines & Bromwich, 2008; Tastula et al., 2012; Valkonen et al., 2014) who attribute this to the Mellor-Yamada-Janjic boundary layer scheme used in the model. The discrepancy in the v component of the wind direction may contribute to explaining the drier air masses in the model, as the more southerly component of the wind in the model will transport air with relatively low moisture content to the area under investigation. King et al. (2015) found a correlation coefficient for water vapor mixing ratio between AMPS data and measurements on the LIS of 0.52. Their study was also based on 6-hourly data but covered only a period of 31 days. We have chosen RH to compare humidity measures in this paper, as this is the parameter delivered by the AWS measurements. If the bias toward a higher wind speed in the model, as presented above, was constant, we would expect a good correlation between model and observations. However, a correlation coefficient for ff of 0.49 indicates that the higher simulated wind speeds tend to occur in episodes. The low correlation coefficient for u (0.28), together with a bias of the same order of magnitude as the one for the scalar wind speed ff, indicates that the model not only overestimates the wind speed along the east-west axis but also tends to overpredict the frequency of occurrence of westerly wind. It misses episodes during which the measurements show an easterly component to the overall wind direction. The very low correlation between measurements and model simulation of v (-0.07) shows that while there is a bias toward more southerly wind direction in the simulation on average, this is not a regular pattern.

Table 2
Average Values and Standard Deviation of Standard Meteorological Parameters as Observed by the AWS at CP (Top) and as Simulated by WRF for AMPS (Bottom)

	T (°C)	p (hPa)	RH (%)	a (g/m^3)	u (m/s)	v (m/s)	ff (m/s)
No Föhn (AWS)	−16.9 ± 8.8	942.9 ± 11.8	97 ± 5	2.9 ± 0.8	2.3 ± 4.0	−1.7 ± 1.5	3.8 ± 3.4
Föhn (AWS)	−0.4 ± 4.9	943.4 ± 11.4	46 ± 13	2.2 ± 0.6	−0.9 ± 2.6	−2.2 ± 2.6	3.4 ± 2.7
Difference (AWS)	**16.5 K**	0.5	**−51**	−0.7	**−3.2**	−0.5	−0.4
No Föhn (AMPS)	−15.3 ± 7.9	942.6 ± 12.0	91 ± 13	1.5 ± 1.0	2.7 ± 2.7	3.0 ± 3.7	5.4 ± 3.0
Föhn (AMPS)	−3.2 ± 4.6	942.7 ± 11.8	60 ± 13	2.3 ± 0.9	7.6 ± 7.2	−4.4 ± 4.5	10.4 ± 7.4
Difference (AMPS)	**12.1 K**	0.1	**−31**	0.8	**4.9**	**−7.4**	**5.0**

Note. Values for non-Föhn data points are shown in the respective top row, values for F Föhn data points in the respective middle row, and the difference between Föhn and non-Föhn is shown in the respective bottom row. Differences in bold are significant at the 99.9 % level.

3.3. Contrasts Between Föhn and Non-Föhn Conditions

In this subsection, we examine the differences between Föhn and non-Föhn conditions at CP in both the observational and model data sets. Table 2 shows how each of the two data sets represents Föhn conditions and non-Föhn conditions through mean values and standard deviations of T, RH, p, wind components u and v, and wind speed ff. It also shows the difference of mean conditions during Föhn and non-Föhn. The differences between Föhn and non-Föhn in the measurements are significant for all parameters except for p, v, and ff. The differences in the model simulations are all significant except that for p. Median values for T are slightly higher than the mean values in all cases. This shows that in case of no Föhn (AWS: −12.2 °C, AMPS: −11.3 °C), there are warm episodes in the area that are not connected to Föhn. In case of Föhn (AWS: 0.2 °C, AMPS: −2.1 °C), it indicates that the temperature distribution is skewed toward higher temperatures in both data sets.

To aid with the interpretation of these differences, Table 3 contains correlation coefficients, biases, and standard deviations between data sets for Föhn and non-Föhn conditions. Correlations of the basic meteorological parameters, which are significant throughout (Table 3), show that—biases apart—the simulations generally follow the course of the observations well. The correlation for all parameters apart from p and v is higher for non-Föhn conditions than for Föhn conditions. In the case of p the difference is negligible (Föhn: 0.99, non-Föhn: 0.98); in case of v the correlation changes sign from positive for Föhn conditions to negative for non-Föhn conditions. This reflects that during Föhn the wind in the observations and the model has a northerly component, while during non-Föhn conditions the wind in the model has a predominantly southerly component.

Observed temperatures at the AWS vary significantly between Föhn and non-Föhn conditions. On average, it is over 16 K warmer under Föhn conditions than when non-Föhn conditions are identified. As Föhn events occur throughout the year, temperatures close to and above freezing can occur during Föhn in all seasons (Kuipers Munneke et al., 2018). The temperature difference in the AMPS data between Föhn and non-Föhn conditions is somewhat smaller, ~12 K. During non-Föhn, the model overestimates the observed temperature by more than 1 K, while it underestimates the temperature during Föhn by almost 3 K.

Table 3
Correlation Coefficients (Upper Row), Bias (Middle Row), and RMSE (Bottom Row) Between Model Simulated and Observational Data for Föhn (Top Half) and No Föhn (Bottom Half)

	T (°C)	p (hPa)	RH (%)	a (g/m^3)	u (m/s)	v (m/s)	ff (m/s)
Föhn ($n = 224$)	**0.90**	**0.99**	**0.34**	**0.49**	**0.45**	**0.45**	**0.53**
	−2.8	−0.7	13	0.1	8.5	−2.2	7.0
	3.55	2.11	20	0.8	10.62	4.62	9.47
no Föhn ($n = 774$)	**0.92**	**0.98**	**0.42**	**0.93**	**0.63**	**−0.43**	**0.67**
	1.6	−0.3	−6	−1.4	0.4	4.7	1.6
	3.72	1.43	13	1.5	3.11	6.52	3.06

Note. Correlations in bold are significant. Listed parameters are temperature T, air pressure p, relative humidity RH, absolute humidity a, vectorial wind speed components u and v, and scalar wind speed ff.

Due to the generally cold climate, the atmosphere in Antarctica in absolute terms is extremely dry. Large differences in RH therefore reflect small changes in absolute humidity. Both data sets show significant differences in mean RH between data points classified as Föhn events and those classified as no Föhn. In the observational data, the difference is 51%, with RH being close to saturation at 97% during no Föhn conditions, and significantly lower at 46% during Föhn. As a RH threshold was used to determine Föhn cases in the observational data, this is to be expected, but the magnitude of the difference is nevertheless an indicator how extremely conditions vary between the two regimes. On average the model simulations result in much lower RH than observed during no Föhn (90%) and significantly more humid air (59%) during Föhn. These numbers show that for both cases simulated RH differs significantly from the observations. Taking the respective mean T values into account, the average absolute moisture content during no Föhn is the same in the observations and the simulations but is significantly higher during Föhn in the model.

The absolute humidity in observations is higher during non-Föhn conditions than during Föhn. The opposite behavior is seen in the simulations, where absolute humidity during Föhn is higher than during non-Föhn conditions. Additionally, the simulated absolute humidity during Föhn is on average lower than that in the observations. Thus, the absolute humidity bias between model and observations is smaller during Föhn than during non-Föhn (see also Figure 3c). This is in contrast to all other parameters except v (Table 3).

The fact that the absolute humidity during Föhn in the model is higher than during non-Föhn, while the opposite is the case for observational data, reflects the biases between model and observations during Föhn and non-Föhn, respectively, in T and RH (Table 1). Both these parameters show significant biases during Föhn from the observations, which are of opposite direction to their respective bias during non-Föhn conditions, such that the model will underestimate the effects of Föhn conditions.

The observations show that on average the wind at the location of the AWS has a westerly component, which is also the case for non-Föhn situations. Interestingly, the observations show a weak, easterly component during Föhn conditions. This can most likely be attributed to the terrain in the vicinity of the AWS. High-resolution simulations with the Unified Model (1.5-km resolution) of a 3 day Föhn event in February 2011 (Elvidge et al., 2015) and simulations with Polar-WRF for a Föhn event in January show that Föhn air flowing across the AP merges with the air flowing off the Antarctic continent over the Ronne Ice Shelf and along the eastern side of the AP. This combined air stream can create an anticyclonic vortex just north of CP, where the airflow is blocked by Jason Peninsula. It is also plausible that Föhn jets flowing down through gaps in the AP mountain range into Mill Inlet to the south of CP and into Cabinet Inlet to the north of CP lead to an easterly counter flow in the lee of CP.

In the modeled data, westerly wind predominates independently of Föhn or no Föhn conditions. While the u-component is of similar magnitude to the observations during non-Föhn, it is much larger during Föhn. Situations when the model simulates an easterly wind component for this location are an exception.

A northerly component prevails in the observational data all through the year and independent of the classification with regard to Föhn conditions. On occasions, southerly wind is observed during Föhn conditions. In the modeled data wind during Föhn events tends to have a northerly component, while during no Föhn on average the wind has a southerly component. Under both conditions the v component of the wind in the model is about twice as large as in the observations.

The average observed wind speed for Föhn events and no Föhn events differs only slightly from the overall average, while, in the model, the wind speed is on average twice as high during non-Föhn than during Föhn conditions. As discussed earlier, in both cases the simulated wind speed is higher than the observed one. Against expectations, the wind speed for both composites, but particularly for all Föhn events, is lower than the overall average wind speed. This indicates that the wind speed observed at the AWS tends to be higher at times when AWS and AMPS data do not agree in their classification with regard to Föhn. This may be connected to the finding that the surface pressure observed at the AWS is on average lower for times when AMPS data and AWS do not agree on their classification with regard to Föhn than when they agree. The poor performance of the model in the simulation of wind speed lies undoubtedly in the complexity of the terrain and the model's relatively coarse spatial resolution (Figure 1). More precisely, by choosing a location within

the model domain that resembles the AWS better with regard to altitude above sea level, we may have inadvertently favored temperature and humidity in the comparison, and disadvantaged wind components, as this location is closer to the spine of the AP.

Figure 3 shows monthly mean values of T, RH, and absolute humidity for Föhn and non-Föhn conditions. As already presented in Table 1 for the entire period under investigation, T and RH are the main parameters characterizing Föhn conditions near the surface. The most striking feature apparent in Figure 3a, in both the observations and model data, is the significantly weaker annual cycle in temperature during Föhn conditions than during non-Föhn conditions. Under non-Föhn conditions, mean temperatures are around -5 °C during the summer months and fall to around -25 °C in the middle of winter, while under Föhn conditions monthly mean temperatures generally lie between -5 and $+5$ °C. This strikingly different seasonal behavior probably reflects the different origins of air masses arriving at CP during Föhn and non-Föhn conditions. During non-Föhn conditions, generally characterized by easterly or southerly flow over the region, air arriving at CP will have originated at low levels over the ice-covered Weddell Sea or the Antarctic continent. Both of these regions are characterized by a large annual cycle in near-surface temperature, which will be reflected in the annual cycle of temperature during non-Föhn conditions at CP. During Föhn conditions, by contrast, air arriving at CP will have originated to the west of the AP Mountains. The mountain chain marks a climate divide between the quasi-continental climate to the east and a more maritime climate, with a much smaller annual cycle in surface temperature to the west (see, e.g., Figure 4 in King et al., 2003). Furthermore, during westerly Föhn, the flow is often blocked at low levels upwind of the AP Mountains, and the air arriving at CP may have originated 500–1,000 m above the surface (Elvidge et al., 2015). Monthly mean temperatures during 2011, taken from the ERA-Interim reanalysis at 1,000 m altitude about 150 km North West of the AP (65.56°S, 66.89°W), are shown in Figure 3a. The annual cycle in these temperatures is much closer to that seen at CP during Föhn conditions than during non-Föhn.

While in general, and under non-Föhn conditions in particular, the model underestimates RH and overestimates T, during Föhn conditions the opposite is the case. The plots in Figure 3 highlight two particular points. First, these biases in T and RH occur throughout the year. Second, the biases are generally larger for Föhn conditions than for non-Föhn cases. Mean T values shown in Figure 3a based on observations reach and exceed freezing regularly during Föhn events. As the values shown are monthly averages, we can assume that temperatures above freezing occur throughout the year during Föhn events. The negative T bias of the model data, evident in Figure 3a, will significantly contribute to the model underestimating the occurrence, frequency, and strength of melt conditions. For mean T during no Föhn conditions the plot shows the generally positive and small model bias, and almost no bias to speak of in the months of August and November. In August a contributing factor to this small bias may be the extremely high number of Föhn events. The bias in January is not representative, as data collection only started on the 22nd of the month. Comparatively small biases in November and December can be explained by the fact that the temperature difference between Föhn and non-Föhn conditions during the austral summer vanishes almost completely, and the main parameter to identify Föhn at this time of year is RH. As the annual cycle in the temperature over the LIS is a lot stronger than that on the more maritime western side of the AP, the effect of the Föhn-induced warming will be much larger during winter with the influx of this maritime air. This opens up two potential reasons for the model's cold bias. One is that AMPS sources the Föhn air on the windward side of the AP from a lower level than it originates from in reality. The second is that AMPS modifies the Föhn air during its descent, for example, by turbulent mixing, more than is the case in reality.

Figure 3b shows a similar pattern for RH as described for T. The bias is larger during Föhn conditions, and it changes sign between Föhn and non-Föhn. During non-Föhn conditions the bias is largest in August, when —due to the low air temperature—the atmosphere is driest. Hence, a small difference in the moisture content of the air can make a big difference in relative terms, especially as the temperature is overestimated in the model, thus increasing the saturation value to which the actual moisture content is related to (Figure 3c).

3.4. The Wider Context

In this section we use the AMPS output over the entire AP region to put the results presented for CP location into a wider context. Figure 4 shows the difference in T 1.5 m between Föhn and non-Föhn for the AP based on AMPS data. It is clearly visible that Föhn conditions have a huge influence on the temperature east of the spine of the AP mountains and far out onto the LIS. Temperature differences are largest at the foot of the
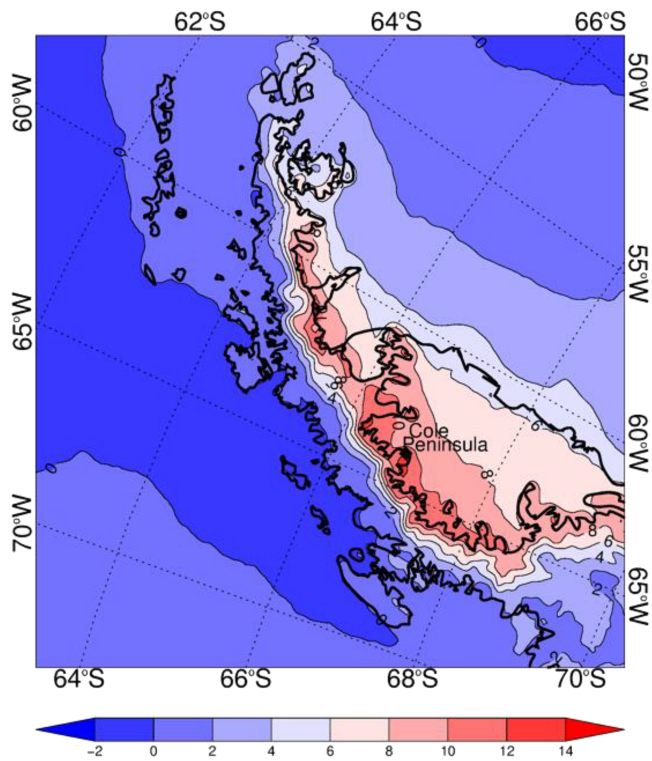
Figure 4. Difference in modeled 1.5 m temperature (K) between composites for Föhn and no Föhn conditions.

mountain range, where in places it is on average up to 14 K warmer during Föhn conditions than under non-Föhn conditions. This extreme difference decreases to 6 K along the edge of the ice shelf and further to 2 K over the Weddell Sea just off the LIS. The west-east gradient in the difference between *T* during Föhn and non-Föhn presented in Figure 4 is supported by observational data presented in Turton et al. (2018). The mean difference of 12.1 K between Föhn and non-Föhn at CP (Table 1) is representative of conditions along the foot of the AP. A few areas on the LIS directly at the foot of the AP, that is, lower than CP, and areas where the topography encourages Föhn jets show higher values. These differences are higher than those presented by King et al. (2017). However, their study was restricted to the melt season from November 2010 to March 2011, and as we have shown, the temperature difference between Föhn and non-Föhn conditions in summer is comparatively low. Taking the same calendar months, but for the period covered in this study (January, February, March, November, and December 2011), AMPS data give an average temperature difference between Föhn and non-Föhn conditions of 3.9 K.

The plots in Figure 5 show mean *RH* for composites of non-Föhn (a) and Föhn (b). During non-Föhn, conditions are on average drier on the western foot of the AP than on the eastern side. During Föhn conditions the eastern side of the AP experiences lower *RH* values, as low as 40%, than the western windward side. Extremely dry areas are found within a narrow band at the foot of the eastern edge of the AP mountains. Again, data for the location of CP are representative for conditions along a large part of the foot of the AP on the LIS.

Figures 6a and 6b show composites of the 10 m wind direction and wind speed for non-Föhn and Föhn, respectively. In the case of non-Föhn conditions, the pressure field shows that the wind direction near the surface is dominantly influenced by a cyclone centered to the southwest of the AP, and a cyclone to the east of the tip of the AP. This synoptic situation leads to more north-easterly wind along the coast on the western side of the AP, and southwesterly wind along the coast on the eastside of the AP. In some areas on the western side, there are indications of gap flows that may be connected with an easterly Föhn. Westerly flow
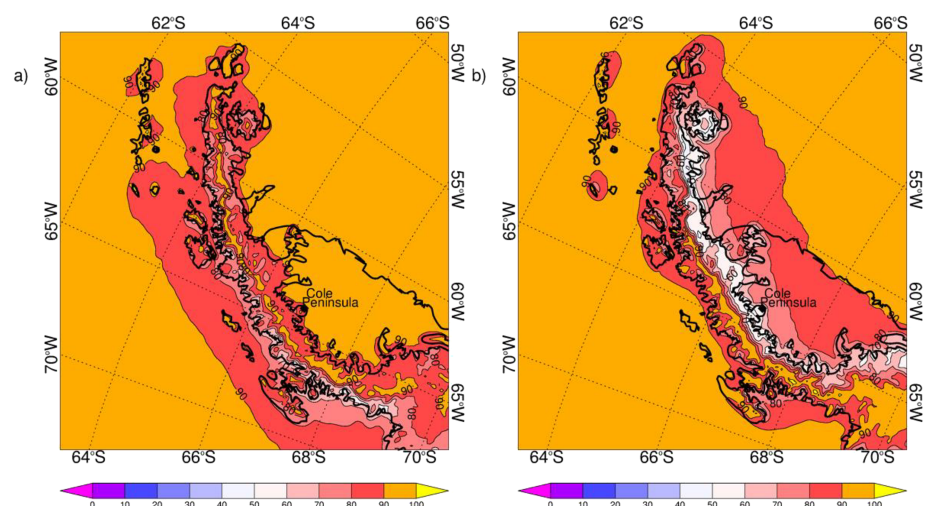

Figure 5. Composite plots of relative humidity with respect to ice for non-Föhn (a) and Föhn (b) conditions based on AMPS data (lowest model level, ~16 m).
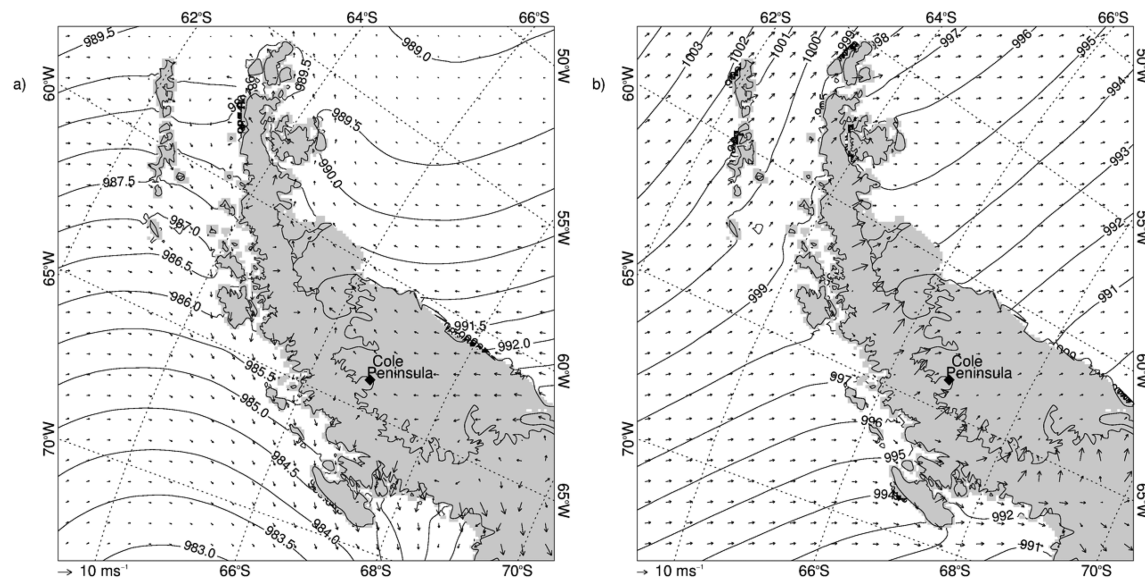
Figure 6. Composite plots of the wind speed and direction at 10 m height (arrows) and surface pressure (contours) for non-Föhn (a) and Föhn (b) conditions during 2011, based on AMPS data.

dominates in the entire region during Föhn conditions (Figure 6b). Extremely strong westerly wind is apparent along most of the leeward side of the AP.

Composite plots of cloud fraction for non-Föhn and Föhn are shown in Figure 7. The strongest signal of Föhn-induced cloud clearing is seen to the east of the LIS over the Weddell Sea rather than in the direct lee of the mountain range. The cloud fraction in the region of CP only reduces by about 10% between non-Föhn and Föhn conditions. The strongest signal with a reduction of up to 30% appears to the east of the LIS over the Weddell Sea. This may explain the comparatively high values of RH near the AP during Föhn in the model, and indicates that more moisture is being retained in the modeled air mass than is the case in reality. King et al. (2015) carried out a 1 month comparison of AMPS surface radiative fluxes with AWS measurements on the LIS and found biases of opposite sign for incoming shortwave (+50 W/m2)
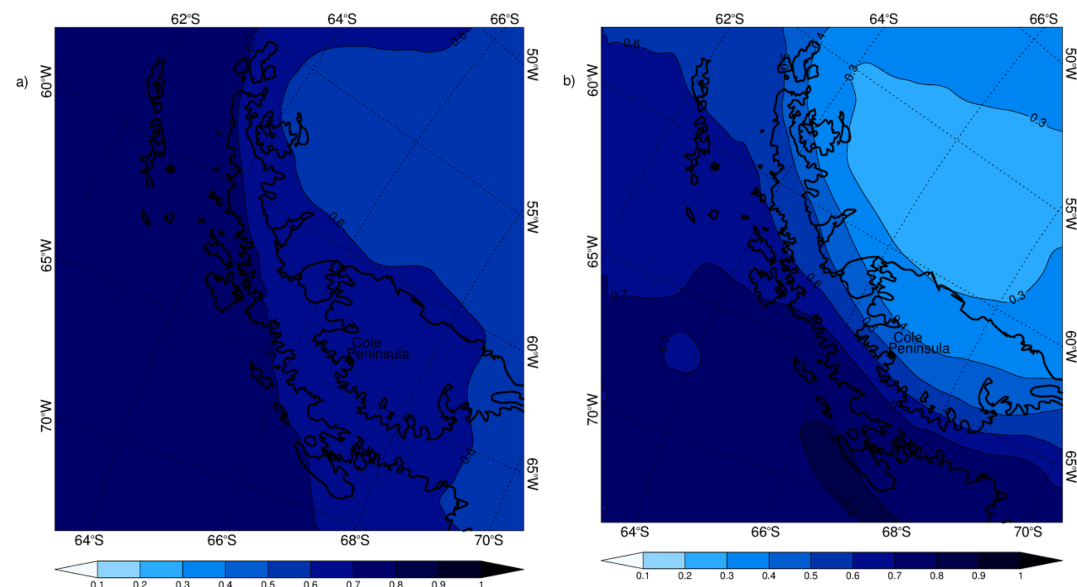

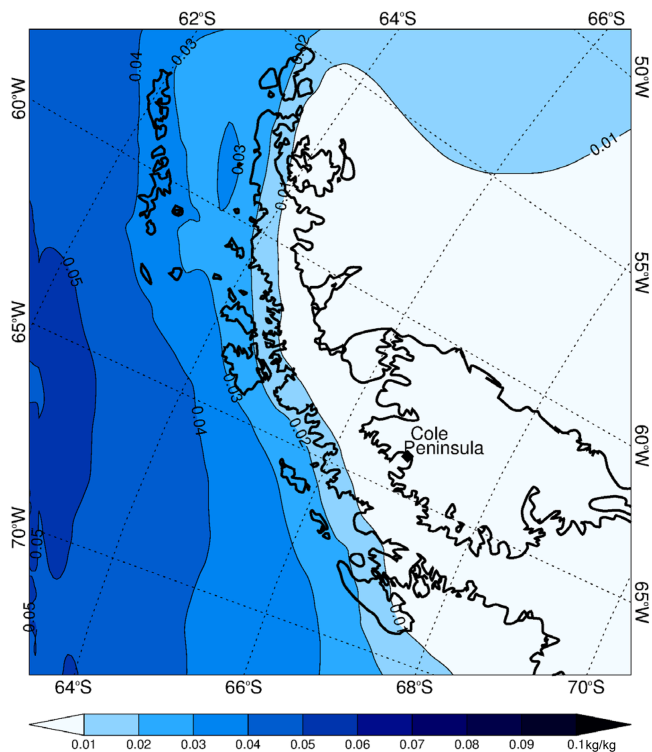**Figure 7.** Composite plots of cloud fraction for non-Föhn (a) and Föhn (b) in AMPS in 2011.

Figure 8. Mean column integrated cloud liquid water during 2011 as simulated by AMPS for all Föhn and non-Föhn cases in 2011 in kilograms per kilogram.

and longwave (−20 W/m2). This suggests that the model's default cloud scheme (WRF single moment 5-class, WSM5) produces low-level clouds that are too optically thin. This is supported by Bromwich et al. (2013) who found an underrepresentation of clouds over Antarctica in Polar WRF when using WSM5. Implementing the Morrison cloud scheme (Morrison et al., 2009) instead of WSM5 improves the model's performance with regard to radiative fluxes over the LIS, significantly reducing the shortwave radiation bias to −5.4 W/m^2, and the longwave radiation bias to +1.3 W/m^2 (C. Listowski, personal communication). A comparison with observations at the British Antarctic Survey's research station at Rothera on the western (windward) side of the AP mountain range though shows that here both cloud schemes produce similar biases to those found over the LIS using WSM5. This implies that independent of the cloud scheme in AMPS, the amount of (low level) clouds on the windward side of the AP is underestimated by AMPS.

As a consequence the effect of Föhn on cloud cover, and hence on T and RH on the leeside of the AP in the model, will be smaller than in the real atmosphere. One potential cause for the smaller effect of Föhn on cloud cover in the model is that AMPS does not simulate any liquid cloud or rain water southwest of a line from 70°S and 75°W to 65°S and ~62°W; that is, all model clouds over our study area are ice clouds, which are optically thinner than liquid water or mixed-phase clouds with the same water content (see Figure 8). Studies by Listowski et al. (2019), Lachlan-Cope et al. (2016), and Grosvenor (2012) have shown that, in reality, a significant amount of liquid water is present in clouds on both sides of the AP, and observations presented by Hines et al. (2019) confirm the presence of liquid water in clouds over West Antarctica which is not adequately simulated by Polar WRF. That the AMPS model does not simulate mixed-phase clouds in this region will particularly affect how low-level clouds, the type of clouds most likely to be influenced by Föhn conditions, are represented.

4. Conclusions

This study investigates the relative quality of AMPS simulations during Föhn in the context of the quality of its simulations during no Föhn. We also provide important observational evidence that Föhn-induced melt conditions frequently occur all year round in the area of the LCIS and are not limited to austral summer, as has been assumed in many previous studies.

As presented in section 3.1, the algorithms that are applied to AWS and AMPS data to identify Föhn conditions lead to good agreement. We can deduce from this that the model satisfactorily reproduces the observed occurrence, frequency, and duration of Föhn events. When discrepancies in these parameters occur, they are predominantly due to one of three reasons: (1) onset or end of Föhn may occur at different times in model and in situ. In most cases our data indicate an offset of 6 hr, that is, one interval between our data points. (2) The threshold for identification as Föhn in AMPS is not reached. (3) The observations do not show Föhn, but AMPS show a Föhn-like signal. This can be caused, for example, by the flow around cyclones that form at the northern tip of the AP and then move into the Weddell Sea area. The model's difficulties to simulate the timing do not have a constant direction, that is, sometimes simulated Föhn starts before the observed event, sometimes it starts later, it seems that different processes are at play here rather than the temporal resolution of the data sets. There is generally good agreement between AMPS simulations and AWS measurements at the location of CP during 2011, as one can see in the general comparison and in the comparison for non-Föhn in Tables 1 and 2. The model does, however, show weaknesses in capturing the strength of Föhn events. This manifests itself in an underestimation of the T increase during Föhn events and in the overestimation of RH during the events.

Particularly noteworthy is that the model slightly overestimates T during non-Föhn, while it significantly underestimates T during Föhn conditions. RH on the contrary is underestimated during non-Föhn and overestimated during Föhn. This is consistent with the findings by King et al. (2017), who, based on model and satellite data combined with observations from the melt season 2010/2011, suggest that AMPS underestimates the sensitivity of the surface energy balance and melt due to Föhn. The model bias for air temperature and relative humidity we find for AMPS overall agrees with that found by Wiesenekker et al. (2018) for the Regional Atmospheric Climate MOdel RACMO, but during Föhn conditions, when our study shows a positive bias for modeled RH (RH higher than observations), the opposite is the case for RH simulated by RACMO in their study.

Over the period studied by King et al. (2015), melt rates simulated by the model were about twice those observed. The bias in net shortwave radiation they report is in equal measures caused by a bias in downwelling SW radiation and an unrealistically low albedo used in the model. This would be consistent with the general overestimation of surface near T in the model we find in this study as well as the lack of cloud water and thus mixed phase clouds.

As T is underestimated during Föhn, the effect of this additional extreme warming on melt conditions over the LCIS will be underestimated in the model. Simulated modeled T in winter never reaches freezing point. Consequently, it is unlikely that the model will be able to reproduce any additional melt during Föhn in winter months adequately (Kuipers Munneke et al., 2018). The overestimation of melt by the model found by King et al. (2015) is caused by shortcomings in the model's shortwave radiation balance. This is only relevant during austral summer and will thus not affect the simulated melt during austral winter when days are very short, and the role of shortwave radiation is negligible. This melt during winter though can be important as it leads to firn air depletion and can precondition the snowpack on the ice shelf for hydrofracturing later on (Kuipers Munneke et al., 2014; Kuipers Munneke et al., 2018). With a projected SAM to shift more into its positive phase in the 21st century (Simpkins & Karpechko, 2012), these winter melt events are likely to occur more often and increase in importance for ice shelf stability.

The model's cold bias during Föhn events has most likely one of two causes. One is that AMPS sources the Föhn air on the windward side of the AP from a lower level than it originates from in reality. The second is that AMPS modifies the Föhn air during its descent, for example, by turbulent mixing, more than is the case in reality. Studying the exact mechanisms causing the Föhn conditions in this area in observations and simulations will contribute to better understanding the causes for this bias.

With regard to the relative humidity, our results indicate that the misrepresentation of cloud properties and particularly the absence of mixed phase clouds in AMPS affects the quality of weather simulation under normal conditions to some extent, and to a larger extent the model's capability to simulate the strength of Föhn conditions adequately.

High-resolution modeling at 1.5 km rather than 5 km resolution improves the representation of Föhn events, for example, with regard to the location of areas of melt, as various case studies that have been analyzed by Elvidge et al. (2015), Elvidge et al. (2016), and Turton et al. (2017). The model resolution used in AMPS for the AP has increased to 3.3 km in 2013 and further to 2.67 km in 2017. While this deals with the complexity of the terrain, this does not address the problems in the model physics that lead to the biases found in this study.

References

Anderson, P. S. (1994). A method for rescaling humidity sensors at temperatures well below freezing. *Journal of Atmospheric and Oceanic Technology*, *11*, 1388–1391.

Anderson, P. S., Mobbs, S., King, J. C., McConnell, I., & Rees, J. (1992). A microbarograph for internal gravity wave studies in Antarctica. *Antarctic Science*, *4*, 241–248.

Banwell, A. F., MacAyeal, D. R., & Sergienko, O. V. (2013). Break-up of the Larsen B Ice Shelf triggered by chain-reaction drainage of supraglacial lakes. *Geophysical Research Letters*, *40*, 5872–5876. https://doi.org/10.1002/2013GL057694

Beran, D. W. (1967). Large amplitude lee waves and chinook winds. *Journal of Applied Meteorology*, *6*, 865–877.

Bromwich, D. H., Otieno, F. O., Hines, K. M., Manning, K. W., & Shilo, E. (2013). Comprehensive evaluation of Polar Weather Research and Forecasting model performance in the Antarctic. *Journal of Geophysical Research: Atmospheres*, *118*, 274–292. https://doi.org/10.1029/2012JD018139

Cape, M. R., Vernet, M., Skvarca, P., Marinsek, S., Scambos, T., & Domack, E. (2015). Foehn winds link climate-driven warming to ice shelf evolution in Antarctica. *Journal of Geophysical Research: Atmospheres*, *120*, 11,037–11,057. https://doi.org/10.1002/2015JD023465

Elvidge, A. D., & Renfrew, I. A. (2016). The causes of foehn warming in the lee of mountains. *Bulletin of the American Meteorological Society*, *97*, 455–466.

Elvidge, A. D., Renfrew, I. A., King, J. C., Orr, A., & Lachlan-Cope, T. A. (2016). Foehn warming distributions in nonlinear and linear flow regimes: A focus on the Antarctic Peninsula. *Quarterly Journal of the Royal Meteorological Society*, *142*, 618–631.

Elvidge, A. D., Renfrew, I. A., King, J. C., Orr, A., Lachlan-Cope, T. A., Weeks, M., & Gray, S. L. (2015). Foehn jets over the Larsen C Ice Shelf, Antarctica. *Quarterly Journal of the Royal Meteorological Society*, *141*, 698–713.

Fogt, R. L., & Bromwich, D. H. (2008). Atmospheric moisture and cloud cover characteristics forecast by AMPS. *Weather and Forecasting*, *23*, 914–930.

Gaffin, D. M. (2007). Foehn winds that produced large temperature differences near the southern Appalachian Mountains. *Weather and Forecasting*, *22*, 145–159.

Grosvenor, D. P., Choularton, T. W., Lachlan-Cope, T., Gallagher, M. W., Crosier, J., Bower, K. N., et al. (2012). In-situ aircraft observations of ice concentrations within clouds over the Antarctic Peninsula and Larsen Ice Shelf. *Atmospheric Chemistry and Physics*, *12*, 11275–11294.

Hines, K. M., & Bromwich, D. H. (2008). Development and testing of Polar Weather Research and Forecasting (WRF) model. Part I: Greenland ice sheet meteorology*. *Monthly Weather Review*, *136*, 1971–1989.

Hines, K. M., Bromwich, D. H., Wang, S. H., Silber, I., Verlinde, J., & Lubin, D. (2019). Microphysics of summer clouds in central West Antarctica simulated by Polar WRF and AMPS. *Atmospheric Chemistry and Physics*, *2019*, 1–48.

Hong, S.-Y., Dudhia, J., & Chen, S.-H. (2004). A revised approach to ice microphysical processes for the bulk parameterization of clouds and precipitation. *Monthly Weather Review*, *132*, 103–120.

Janjic, Z. I. (1994). The step-mountain eta coordinate model: Further developments of the convection, viscous sublayer, and turbulence closure schemes. *Monthly Weather Review*, *122*, 927–945.

King, J. C., Gadian, A., Kirchgaessner, A., Kuipers Munneke, P., Lachlan-Cope, T. A., Orr, A., et al. (2015). Validation of the summertime surface energy budget of Larsen C Ice Shelf (Antarctica) as represented in three high-resolution atmospheric models. *Journal of Geophysical Research: Atmospheres*, *120*, 1335–1347. https://doi.org/10.1002/2014JD022604

King, J. C., Kirchgaessner, A., Bevan, S., Elvidge, A. D., Kuipers Munneke, P., Luckman, A., et al. (2017). The impact of Föhn winds on surface energy balance during the 2010–2011 melt season over Larsen C Ice Shelf, Antarctica. *Journal of Geophysical Research: Atmospheres*, *122*, 12,062–12,076. https://doi.org/10.1002/2017JD026809

King, J. C., Turner, J., Marshall, G. J., Connolley, W. M., & Lachlan-Cope, T. A. (2003). Antarctic Peninsula climate variability and its causes as revealed by analysis of instrumental records. *Antarctic Research Series*, *79*, 17–30.

Kuipers Munneke, P., Ligtenberg, S. R. M., Van Den Broeke, M. R., & Vaughan, D. G. (2014). Firn air depletion as a precursor of Antarctic ice-shelf collapse. *Journal of Glaciology*, *60*, 205–214.

Kuipers Munneke, P., Luckman, A. J., Bevan, S. L., Smeets, C. J. P. P., Gilbert, E., van den Broeke, M. R., et al. (2018). Intense winter surface melt on an Antarctic ice shelf. *Geophysical Research Letters*, *45*, 7615–7623. https://doi.org/10.1029/2018GL077899

Lachlan-Cope, T., Listowski, C., & O'Shea, S. (2016). The microphysics of clouds over the Antarctic Peninsula—Part 1: Observations. *Atmospheric Chemistry and Physics*, *16*, 15605–15617.

Listowski, C., Delanoë, J., Kirchgaessner, A., Lachlan-Cope, T., & King, J. (2019). Antarctic clouds, supercooled liquid water and mixed phase, investigated with DARDAR: Geographical and seasonal variations. *Atmospheric Chemistry and Physics*, *19*, 6771–6808.

Marshall, G. J. (2003). Trends in the Southern Annular Mode from observations and reanalyses. *Journal of Climate*, *16*, 4134–4143.

Marshall, G. J., Orr, A., Lipzig, N. P. M. V., & King, J. C. (2006). The impact of a changing Southern Hemisphere annular mode on Antarctic Peninsula summer temperatures. *Journal of Climate*, *19*, 5388–5404.

Massom, R. A., Scambos, T. A., Bennetts, L. G., Reid, P., Squire, V. A., & Stammerjohn, S. E. (2018). Antarctic ice shelf disintegration triggered by sea ice loss and ocean swell. *Nature*, *558*, 383–389.

McGrath, D., Steffen, K., Rajaram, H., Scambos, T., Abdalati, W., & Rignot, E. (2012). Basal crevasses on the Larsen C Ice Shelf, Antarctica: Implications for meltwater ponding and hydrofracture. *Geophysical Research Letters*, *39*, L16504. https://doi.org/10.1029/2012GL052413

Morrison, H., Thompson, G., & Tatarskii, V. (2009). Impact of cloud microphysics on the development of trailing stratiform precipitation in a simulated squall line: Comparison of one- and two-moment schemes. *Monthly Weather Review*, *137*, 991–1007.

Orr, A., Marshall, G. J., Hunt, J. C. R., Sommeria, J., Wang, C. G., van Lipzig, N. P. M., et al. (2008). Characteristics of summer airflow over the Antarctic Peninsula in response to recent strengthening of westerly circumpolar winds. *Journal of the Atmospheric Sciences*, *65*(4), 1396–1413. https://doi.org/10.1175/2007JAS2498.1

Powers, J. G., Manning, K. W., Bromwich, D. H., Cassano, J. J., & Cayette, A. M. (2012). A decade of Antarctic science support through AMPS. *Bulletin of the American Meteorological Society*, *93*, 1699–1712.

Powers, J. G., Monaghan, A. J., Cayette, A. M., Bromwich, D. H., Kuo, Y.-H., & Manning, K. W. (2003). Real-time mesoscale modeling over Antarctica: The Antarctic Mesoscale Prediction System*. *Bulletin of the American Meteorological Society*, *84*, 1533–1545.

Richner, H., Baumann-Stanzer, K., Benech, B., Berger, H., Chimani, B., Dorninger, M., et al. (2006). Unstationary aspects of foehn in a large valley part I: Operational setup, scientific objectives and analysis of the cases during the special observing period of the MAP subpro- gramme FORM. *Meteorology and Atmospheric Physics*, *92*, 255–284.

Richner, H., & Hächler, P. (2013). Understanding and forecasting Alpine foehn. In K. F. Chow, F. J. S. de Wekker, & J. B. Snyder (Eds.), *Mountain Weather Research and Forecasting: Recent Progress and Current Challenges* (pp. 219–260). Dordrecht: Springer.

Scambos, T., Hulbe, C., & Fahnestock, M. (2003). Climate-induced ice shelf disintegration in the Antarctic Peninsula. *Antarctic Peninsula climate variability: Historical and paleoenvironmental perspectives*, *79*, 79–92.

Scambos, T. A., Bohlander, J. A., Shuman, C. A., & Skvarca, P. (2004). Glacier acceleration and thinning after ice shelf collapse in the Larsen B embayment, Antarctica. *Geophysical Research Letters*, *31*, L18402. https://doi.org/10.1029/2004GL020670

Seefeldt, M. W., & Cassano, J. J. (2008). An analysis of low-level jets in the greater Ross Ice Shelf region based on numerical simulations. *Monthly Weather Review*, *136*, 4188–4205.

Simpkins, G. R., & Karpechko, A. Y. (2012). Sensitivity of the southern annular mode to greenhouse gas emission scenarios. *Climate Dynamics*, *38*, 563–572.

Skamarock, W., Klemp, J. B., Dudhia, J., Gill, D. O., Barker, D., Duda, M. G., et al. (2008). A description of the advanced research WRF version 3. Technical Notes NCAR/TN-4751STR, 113 pp.

Smith, R. (1990). Why can't stably stratified air rise over high ground. *Atmospheric Processes over Complex Terrain, Meteor. Monogr*, 105–107.

Speirs, J. C., Steinhoff, D. F., McGowan, H. A., Bromwich, D. H., & Monaghan, A. J. (2010). Foehn winds in the McMurdo dry valleys, Antarctica: The origin of extreme warming events*. *Journal of Climate*, *23*, 3577–3598.

Steinhoff, D. F., Bromwich, D. H., Speirs, J. C., McGowan, H. A., & Monaghan, A. J. (2014). Austral summer foehn winds over the McMurdo dry valleys of Antarctica from Polar WRF. *Quarterly Journal of the Royal Meteorological Society*, *140*, 1825–1837.

Steinhoff, D. F., Chaudhuri, S., & Bromwich, D. H. (2009). A case study of a Ross Ice Shelf airstream event: A new perspective. *Monthly Weather Review*, *137*, 4030–4046.

Tastula, E.-M., Vihma, T., & Andreas, E. L. (2012). Evaluation of Polar WRF from modeling the atmospheric boundary layer over Antarctic sea ice in autumn and winter. *Monthly Weather Review*, *140*, 3919–3935.

Turner, J., Colwell, S. R., Marshall, G. J., Lachlan-Cope, T. A., Carleton, A. M., Jones, P. D., et al. (2005). Antarctic climate change during the last 50 years. *International Journal of Climatology*, *25*(3), 279–294. https://doi.org/10.1002/joc.1130

Turton, J. V., Kirchgaessner, A., Ross, A. N., & King, J. C. (2017). Does high-resolution modelling improve the spatial analysis of föhn flow over the Larsen C Ice Shelf? *Weather*, *72*, 192–196.

Turton, J. V., Kirchgaessner, A., Ross, A. N., & King, J. C. (2018). The spatial distribution and temporal variability of föhn winds over the Larsen C Ice Shelf, Antarctica. *Quarterly Journal of the Royal Meteorological Society*, *144*, 1169–1178.

Valkonen, T., Vihma, T., Johansson, M. M., & Launiainen, J. (2014). Atmosphere–sea ice interaction in early summer in the Antarctic: Evaluation and challenges of a regional atmospheric model. *Quarterly Journal of the Royal Meteorological Society*, *140*, 1536–1551.

van Lipzig, N. P. M., Marshall, G. J., Orr, A., & King, J. C. (2008). The relationship between the Southern Hemisphere annular mode and Antarctic Peninsula summer temperatures: Analysis of a high-resolution model climatology. *Journal of Climate*, *21*, 1649–1668.

Vaughan, D. G., Marshall, G. J., Connolley, W. M., King, J. C., & Mulvaney, R. (2001). Devil in the detail. *Science*, *293*, 1777–1779.

Vázquez, B. G. E., & Grejner-Brzezinska, D. A. (2013). GPS-PWV estimation and validation with radiosonde data and numerical weather prediction model in Antarctica. *GPS Solutions*, *17*, 29–39.

Wiesenekker, J., Kuipers Munneke, P., van den Broeke, M., & Smeets, C. (2018). A multidecadal analysis of Föhn winds over Larsen C Ice Shelf from a combination of observations and modeling. *Atmosphere*, *9*, 172.

Wille, J. D., Bromwich, D. H., Nigro, M. A., Cassano, J. J., Mateling, M., Lazzara, M. A., & Wang, S.-H. (2016). Evaluation of the AMPS boundary layer simulations on the Ross Ice Shelf with tower observations. *Journal of Applied Meteorology and Climatology*, *55*, 2349–2367.